Sandwiched Electrochemiluminescent Peptide Biosensor for the Detection of Prognostic Indicator in Early-Stage Cancer Based on Hollow, Magnetic, and Self-Enhanced Nanosheets

Haijun Wang, Yali Yuan, Yaqin Chai, and Ruo Yuan**

Currently, peptide-based protein-recognition has been recognized as an effective and promising approach for protein assays. However, sandwiched peptide-based biosensor with high sensitivity and low background has not been proposed before. Herein, a sandwiched electrochemiluminescence (ECL) peptide-based biosensor is constructed for Cyclin A_2 (CA2), a prognostic indicator in early stage of multiple cancers, based on nanosheets with hollow, magnetic, and ECL self-enhanced properties. First, hollow and magnetic manganese oxide nanocrystals (H-Mn_3O_4) are synthesized using triblock copolymeric micelles with core–shell–corona architecture as templates. Then, polyethyleneimine (PEI) and the composite of platinum nanoparticles and tris (4,4′-dicarboxylicacid-2,2′-bipyridyl) ruthenium (II) (PtNPs–Ru) are immobilized on H-Mn_3O_4 to form H-Mn_3O_4–PEI–PtNPs–Ru nanocomposite, in which PEI as coreactant can effectively enhance the luminous efficiency and PtNPs as nanochannels can greatly accelerate the electron transfer. Finally, due to the coordination between Eu^{3+} and carboxyl, the obtained H-Mn_3O_4–PEI–PtNPs–Ru aggregates locally to form sheet-like nanostructures ((H-Mn_3O_4–PEI–PtNPs–Ru)$_n$–Eu^{3+}), by which the luminous efficiency is further increased. Based on the nanosheets and two designed peptides, a sandwiched ECL biosensor, using palladium nanocages synthesized through galvanic replacement reaction as substrate, is proposed for CA2 with a linear range from 0.001 to 100 ng mL^{-1} and a detection limit of 0.3 pg mL^{-1}.

1. Introduction

Up to now, antibody-based protein-recognition is a common approach in the quantitative immunological assay for target proteins.[1,2] Nevertheless, this technique has some drawbacks for protein analysis, for instance, the requirement of producing high-quality antibodies, low capacity for multiplexed analyte detection, the difficulty in site-specific bioconjugation and maintaining the initial activity.[3–5] Furthermore, signal amplifiers usually require multiple steps for preparation when an antibody-based biosensor is fabricated because antibodies have multiple domains and complicated glycosylation patterns. In this occasion, more and more interests are gradually focused on new methods for protein assay. Peptides, with simple and defined structure, exhibit specific and strong affinity for many molecular partners, including proteins, cells, nucleic acid, and small molecules.[6,7] Moreover, peptides possess a great many advantages, including simplicity, versatility, accessibility, chemical definition, cost effectiveness, etc.[8,9] Herein, peptide-based molecule recognition is becoming an

Dr. H. Wang, Y. Yuan, Prof. Y. Chai, R. Yuan
Key Laboratory of Luminescent and Real-Time Analytical Chemistry
Ministry of Education
College of Chemistry and Chemical Engineering
Southwest University
Chongqing 400715, P. R. China
E-mail: yqchai@swu.edu.cn; yuanruo@swu.edu.cn

DOI: 10.1002/smll.201500321

important and promising candidate for biological analysis.[10] However, most of the existing peptide-based biosensors are constructed with label-free model which have limitation in the sensitivity. As a classic and effective form in the fabrication of sensor, sandwich-tape biosensor has advantages in low background signal, easy labeling, and high detection sensitivity.[11] Therefore, exploring the peptide-based biosensor with sandwiched recognition and "signal-on" model is very necessary.

Cyclins are key proteins during the cell cycle, whose overexpression will lead to cancerization of cell accompany with uncontrolled cell division and proliferation. Cyclin A_2 (CA2), a globular protein, is an important member of the super cyclin family. Through the association of cyclin-dependent kinases (CDK), CA2 participates in DNA replication, transcription, and regulates cell cycle.[12,13] It has been reported that CA2 over expresses in many types of cancers including liver cancer, breast cancer, lung cancer, lymphoma, leukemia, etc.[14,15] Thusness, CA2 can be served as a prognostic indicator in early-stage cancer and a promising anticancer target for the development of tumor therapeutic agents.[16] Therefore, developing a simple, sensitive, selective analytical method for CA2 is significant for clinical diagnosis and treatment of cancer in the early stage. Due to the cyclin binding groove (CBG) (the amino acid subsequences of (210, 211, 372, 217, 218, 220, 221, 243, 253, 254)), CA2 can be specifically recognized by the well-known peptide with consensus sequence of Arg/Lys–Xaa–Leu where Xaa is any amino acid.[17,18] Furthermore, according to the GenBank, CA2 has binding sites at the amino acid subsequences of (361, 365, 372, 387, 390, 391). Accordingly, two peptides for selective recognition of CA2 are designed to construct a sandwiched "signal-on" biosensor. To our best knowledge, little research about this area has been reported.

As a sensitive technique, electrochemiluminescence (ECL) has attracted considerable attention due to its integrated advantages of electrochemistry and chemiluminescence.[19–21] Currently, ECL has been applied in many areas, for instance, immunoassay, DNA detection, pharmaceutical analysis, clinical diagnosis, environmental analysis, etc.[22–24] In those applications, the key aspect in the construction of ECL-based biosensors is how to accomplish the signal amplification. Introducing the coreactants into ECL system is a usually used method.[25,26] However, different introducing ways will receive different amplified effect. For example, owing to their biological toxicity and volatile nature, some coreactants that are directly put into the detection solution will sophisticate the operation, increase the measurement error and the used amount of reagent.[27] Furthermore, the relaxation effect while the coreactants diffuse to the electrode surface is usually accompanied with loss of energy, which will lead to the decrease of luminous efficiency. Thus, we focus on how to enhance the reacted efficiency between the luminescent reagent and corresponding coreactants in the further research. In this work, self-enhanced nanostructures that included the luminophore and the corresponding coreactant in the same complex were synthetized. Furthermore, platinum nanoparticles (PtNPs), with excellent conductivity and biological compatibility, are used as nanochannels between the luminescent reagent and corresponding coreactant, by which the electron transfer rate is accelerated, and the luminous stability and efficiency are enhanced.

Because of their excellent properties, nanomaterials are widely applied in the bioanalysis based on ECL.[28–30] And increasing interest has been focused on hollow nanostructures owing to their relatively lower densities, larger specific surface areas, better mechanical and thermal stabilities.[31–33] Using sacrificial templates to prepare such hollow nanostructures has proven to be successful. For example, cage-like nanostructures, with hollow interiors and porous walls, can be synthesized by galvanic replacement reactions with silver nanocubes acting as templates.[34,35] Due to their upstanding properties in specific surface areas, electrocatalytic activity, and biocompatibility, the obtained nanocages can serve as good potential candidates for the fabrication of biosensors. Recently, the triblock copolymeric micelles of poly(styreneb-2-vinyl pyridine-*b*-ethylene oxide) (PS-PVP-PEO) with core–shell–corona (CSC) architecture are proposed as soft templates for the synthesis of inorganic hollow nanoparticles.[36,37] The hydrophobic PS core acts as a template of the hollow. The ionizable hydrophilic PVP shell selectively reserves the inorganic precursors. The hydrophilic PEO corona can prevent the structure form aggregation and enhance the stability. Compared to the hard templates, they have superiorities in size control, product yield, and template removal. Therefore, this method will have promising application in the synthesis of nanomaterials with hollow structure.

In this work, two specific peptides for selective recognition of CA2 are designed first, and the binding schematic diagram between CA2 and the two specific peptides is showed in **Scheme 1**. Then, hollow and magnetic manganese oxide nanocrystals (H-Mn_3O_4) were synthetized by using CSC polymeric templates. Polyethyleneimine (PEI) and the composite of platinum nanoparticles and tris (4,4′-dicarboxylicacid-2,2′-bipyridyl) ruthenium (II) dichloride (PtNPs–Ru) were well chemically decorated on the surface of obtained H-Mn_3O_4 due to the high specific surface areas. In the presence of Eu^{3+}, the prepared nanocomposite (H-Mn_3O_4–PEI–PtNPs–Ru) above aggregated locally together to form sheet-like nanostructure ((H-Mn_3O_4–PEI–PtNPs–Ru)$_n$–Eu^{3+}). Besides the special nanostructure and good magnetism, the nanosheets possessed outstanding ECL performance because the

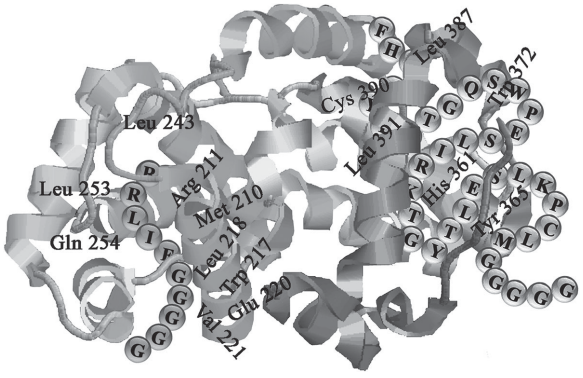

Scheme 1. The binding schematic diagram between CA2 and the two specific peptides.

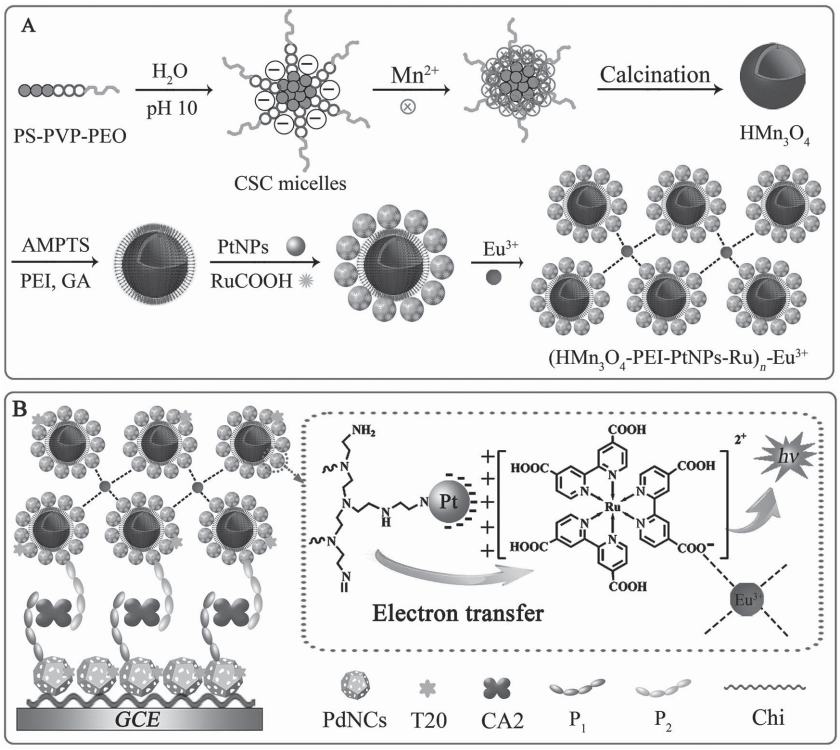

Scheme 2. A) The preparation of H-Mn_3O_4 and (H-Mn_3O_4–PEI–PtNPs–Ru)$_n$–Eu^{3+}; B) the preparation and amplification mechanism of ECL biosensor.

coreactant (PEI) and the luminescent reagent (Ru complexes) existed in the same nanostructure with PtNPs acting as nanochannels for electron transfer between them. Whereafter, the nanosheets were used to immobilize the detection peptide with Tween 20 (T20) preventing nonspecific binding. In addition, palladium nanocages (PdNCs), with high specific surface areas and good biocompatibility, were synthesized through a galvanic replacement reaction and applied to immobilize the capture peptide. Based on the specific recognition of cyclin-peptide to CA2, a "signal-on" peptide-based ECL biosensor was fabricated for the detection of CA2 (the preparation of the materials and the biosensor is showed in **Scheme 2**).

2. Results and Discussion

2.1. Morphologies and Elements Analysis of the Different Nanomaterials

The morphologies of different nanomaterials prepared in this work were monitored by scanning electron microscopy (SEM, **Figure 1**) and transmission electron microscope (TEM, Figure S1, Supporting Information). The morphologies of PdNCs were showed in Figure 1A and Figure S1A, Supporting Information, which suggested that a large number of particles stacked cages were clearly observed. With using silver nanocubes as templates, the obtained PdNCs retained partial cubic prototype. By using CSC polymeric micelles as soft templates, the obtained H-Mn_3O_4 had obvious hollow structure (Figure 1B and Figure S1B, Supporting Information). After the modification of PEI and PtNPs–Ru composite, abundant of nanoparticles adsorbed H-Mn_3O_4 appeared (Figure 1C and Figure S1C, Supporting Information). Finally, H-Mn_3O_4 adsorbed with abundant of nanoparticles aggregated locally to form sheet-like nanostructure owing to the coordination between Eu^{3+} and carboxyl (Figure 1D and Figure S1D, Supporting Information).

Furthermore, XPS was performed for the elemental analysis of (H-Mn_3O_4–PEI–PtNPs–Ru)$_n$–Eu^{3+} composite. As shown in **Figure 2**, the peaks at 284.7, 399.8, 485.2, and 531.4 eV could be, respectively, assigned to C1s, N1s, Ru3p, and O1s XPS spectra, which suggested the presence of PEI and Ru luminophore. In addition, the XPS doublets of Pd4f (84.0 and 88.9 eV), Mn2p (641.5 and 653.4 eV), Eu3d (1134.6 and 1165.9 eV) indicated the existence of the PtNPs, H-Mn_3O_4, and Eu^{3+}, respectively. Based on the elemental analysis results above, we could ensure that the (H-Mn_3O_4–PEI–PtNPs–Ru)$_n$–Eu^{3+} composite was successfully prepared.

2.2. Magnetic Properties of the Prepared Materials

For magnetic materials, maintaining the inherent magnetic properties is very important. In our experiments, the magnetic properties of H-Mn_3O_4 and (H-Mn_3O_4–PEI–PtNPs–Ru)$_n$–Eu^{3+} composite were measured. As shown in **Figure 3**, the saturated specific magnetization of H-Mn_3O_4 was about 0.08 emu g^{-1}. Then, the saturated specific magnetization of (H-Mn_3O_4–PEI–PtNPs–Ru)$_n$–Eu^{3+} decreased to about 0.05 emu g^{-1}. This decrease may be due to the fact that PEI, PtNPs, and Ru luminophore were nonmagnetic materials, which could decrease the saturated specific magnetization. In

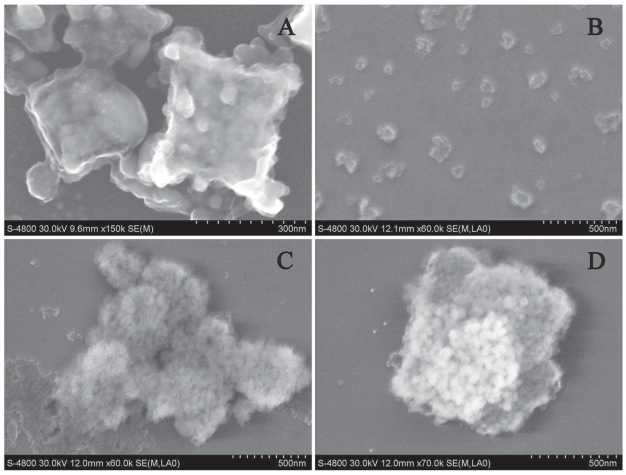

Figure 1. SEM images of A) PdNCs, B) H-Mn_3O_4, C) H-Mn_3O_4–PEI–PtNPs–Ru, D) (H-Mn_3O_4–PEI–PtNPs–Ru)$_n$–Eu^{3+}.

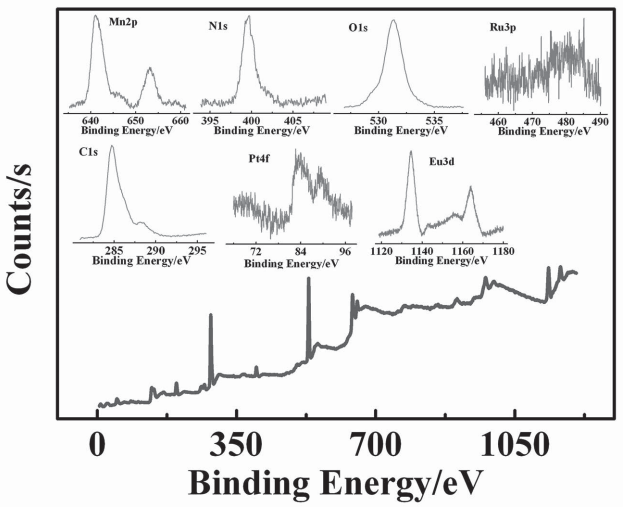

Figure 2. XPS analysis for the full region of XPS for $(H\text{-}Mn_3O_4\text{–}PEI\text{–}PtNPs\text{–}Ru)_n\text{–}Eu^{3+}$.

conclusion, the composite of $(H\text{-}Mn_3O_4\text{–}PEI\text{–}PtNPs\text{–}Ru)_n\text{–}Eu^{3+}$ with good magnetism was successfully synthesized, which could be easily separated in the follow-up modification with assistance of an external magnet.

2.3. Characterization of the ECL Biosensor

In order to prove the feasibility of the sandwiched recognition for CA2 based on the two peptides, enzyme linked immunosorbent assay (ELISA) was performed (Figure S2, Supporting Information). Furthermore, the proposed biosensor was characterized by ECL in PBS (0.1 M, pH 7.4). As shown in **Figure 4**A, there is almost no ECL response before the incubation of $(H\text{-}Mn_3O_4\text{–}PEI\text{–}PtNPs\text{–}Ru)_n\text{–}Eu^{3+}@P_2\text{-}T20$ bioconjugate (black curve) due to inexistence of ECL luminophore. However, an obvious ECL signal appeared when $(H\text{-}Mn_3O_4\text{–}PEI\text{–}PtNPs\text{–}Ru)_n\text{–}Eu^{3+}@P_2\text{-}T20$ was immobilized on the electrode, which suggested the successful modification of $(H\text{-}Mn_3O_4\text{–}PEI\text{–}PtNPs\text{–}Ru)_n\text{–}Eu^{3+}@P_2\text{-}T20$ bioconjugate (red curve).

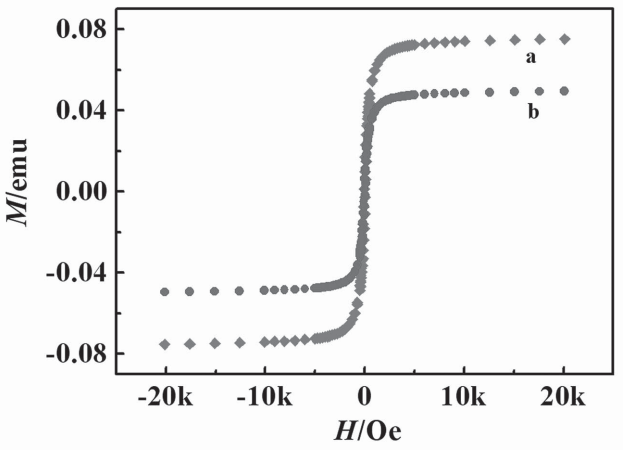

Figure 3. Room-temperature magnetic-hysteresis loop for the $H\text{-}Mn_3O_4$ (a) and $(H\text{-}Mn_3O_4\text{–}PEI\text{–}PtNPs\text{–}Ru)_n\text{–}Eu^{3+}$ (b).

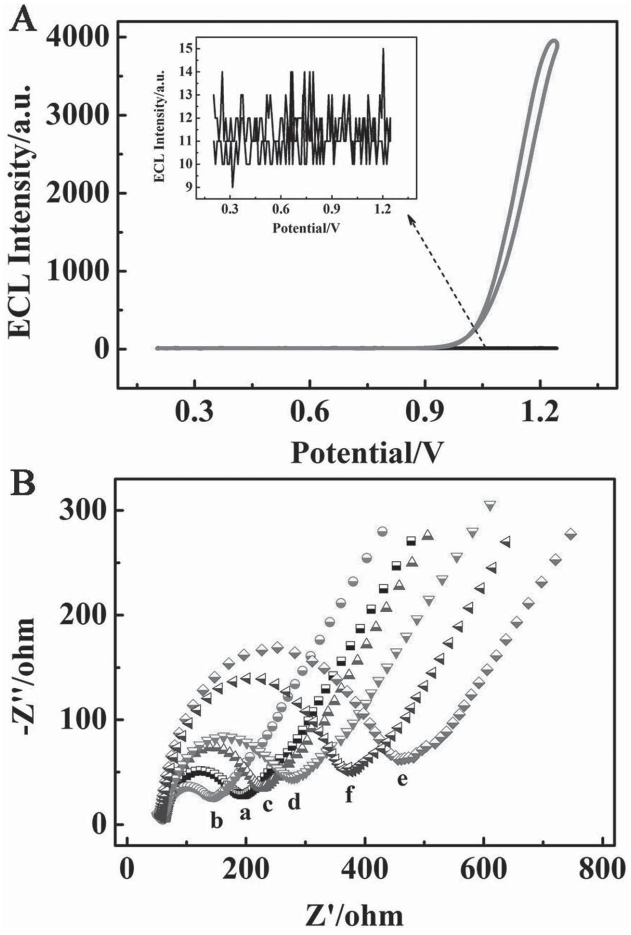

Figure 4. A) ECL profiles of the biosensor in 20 ng mL^{-1} CA2 before (black curve) and after (red curve) the modification of $(H\text{-}Mn_3O_4\text{–}PEI\text{–}PtNPs\text{–}Ru)_n\text{–}Eu^{3+}@P_2\text{-}T20$ bioconjugate; B) EIS profiles of (a) Bare GCE, (b) GCE/PdNCs, (c) GCE/PdNCs/P_1, (d) GCE/PdNCs/P_1/T20, (e) GCE/PdNCs/P_1/T20/CA2, (f) GCE/PdNCs/P_1/T20/CA2/$(H\text{-}Mn_3O_4\text{–}PEI\text{–}PtNPs\text{–}Ru)_n\text{–}Eu^{3+}@P_2\text{-}T20$ in 5×10^{-3} M $[Fe(CN)_6]^{3-/4-}$ containing 0.1 M KCl.

Meanwhile, electrochemical impedance spectroscopy (EIS) was performed to characterize the stepwise fabrication process of the ECL biosensor in 5×10^{-3} M $[Fe(CN)_6]^{3-/4-}$ containing 0.1 M KCl. As shown in Figure 4 B, the bare GCE had a small semicircle in the base solution (curve a). Then, a decreased impedance value was obtained after the modification of PdNCs owing to its outstanding electric conductivity (curve b). After the successive immobilization of P_1, T20, CA2 (20 ng mL^{-1}), the impedance values increased in order (curve c–e). That was because the formation of protein molecules layers hindered the electron transfer. However, after the incubation of $(H\text{-}Mn_3O_4\text{–}PEI\text{–}PtNPs\text{–}Ru)_n\text{–}Eu^{3+}@P_2\text{-}T20$ bioconjugate, the impedance value was reduced (curve f), which could be ascribe to the fact that the materials in the bioconjugate promoted the electron transfer.

2.4. Comparison of the Biosensor with Different P_2 Bioconjugates

Five kinds of P_2 bioconjugates were prepared to illustrate the advantages of the biosensor with the target

bioconjugate: (a) $(H\text{-}Mn_3O_4\text{–}PEI\text{–}PtNPs\text{–}Ru)_n\text{–}Eu^{3+}@P_2\text{-}T20$ (target bioconjugate), (b) $(H\text{-}Mn_3O_4\text{–}PEI\text{–}Ru)_n\text{–}Eu^{3+}@P_2\text{-}T20$, (c) $(PEI\text{–}PtNPs\text{–}Ru)_n\text{–}Eu^{3+}@P_2\text{-}T20$, (d) $H\text{-}Mn_3O_4\text{–}PEI\text{–}PtNPs\text{–}Ru@P_2\text{-}T20$, and (e) $(H\text{-}Mn_3O_4\text{–}PtNPs\text{–}Ru)_n\text{–}Eu^{3+}@P_2\text{-}T20$. The same batch of biosensors were prepared and incubated with 20 ng mL^{-1} CA2, then incubated with different P_2 bioconjugate solutions, respectively. The changed values of the ECL responses (ΔI) of the biosensor with different bioconjugates were showed in Figure S3, Supporting Information. The ΔI of the biosensor with target bioconjugate was 3950.4 a.u. (Figure S3A, Supporting Information). Then, the ΔI were decreased to 2450.3, 2108.9, 1797.3, and 838.6 a.u. when the biosensor was incubated with $(H\text{-}Mn_3O_4\text{–}PEI\text{–}Ru)_n\text{–}Eu^{3+}@P_2\text{-}T20$, $(PEI\text{–}PtNPs\text{–}Ru)_n\text{–}Eu^{3+}@P_2\text{-}T20$, $H\text{-}Mn_3O_4\text{–}PEI\text{–}PtNPs\text{–}Ru@P_2\text{-}T20$, and $(H\text{-}Mn_3O_4\text{–}PtNPs\text{–}Ru)_n\text{–}Eu^{3+}@P_2\text{-}T20$, respectively (Figures S3B–E, Supporting Information). The reason could be as follows: First, PtNPs, with excellent electrocatalytic ability could act as nanochannels for electron transfer and energy transmission and enhanced the ECL signal. Second, $H\text{-}Mn_3O_4$ with hollow structure had high specific surface areas, which could load increased amount of luminescent reagent and coreactant. Third, the loading amounts of $H\text{-}Mn_3O_4$, PEI, PtNPs, and Ru luminophore further increased due to the coordination of Eu^{3+}. Finally, PEI as an effective coreactant to Ru luminophore had remarkable influence to the final ECL signal, especially in a self-enhanced composite.

2.5. The Possible Luminous Mechanisms of $(H\text{-}Mn_3O_4\text{–}PEI\text{–}PtNPs\text{–}Ru)_n\text{–}Eu^{3+}$ Composite

The possible mechanisms to the ECL of $(H\text{-}Mn_3O_4\text{–}PEI\text{–}PtNPs\text{–}Ru)_n\text{–}Eu^{3+}$ were described with the following equations

$$\left(H\text{-}Mn_3O_4\text{-}PEI\text{-}PtNPs\text{-}Ru(II)\right)_n\text{-}Eu^{3+} - 2e \rightarrow \left(H\text{-}Mn_3O_4\text{-}PEI^{\bullet+}\text{-}PtNPs\text{-}Ru(III)\right)_n\text{-}Eu^{3+} \quad (1)$$

$$\left(H\text{-}Mn_3O_4\text{-}PEI^{\bullet+}\text{-}PtNPs\text{-}Ru(III)\right)_n\text{-}Eu^{3+} \rightarrow \left(H\text{-}Mn_3O_4\text{-}PEI^{\bullet}\text{-}PtNPs\text{-}Ru(III)\right)_n\text{-}Eu^{3+} + H^+ \quad (2)$$

$$\left(H\text{-}Mn_3O_4\text{-}PEI^{\bullet}\text{-}PtNPs\text{-}Ru(III)\right)_n\text{-}Eu^{3+} \rightarrow \left(H\text{-}Mn_3O_4\text{-}PEI\text{-}PtNPs\text{-}Ru^{*}(II)\right)_n\text{-}Eu^{3+} \quad (3)$$

$$\left(H\text{-}Mn_3O_4\text{-}PEI\text{-}PtNPs\text{-}Ru^{*}(II)\right)_n\text{-}Eu^{3+} \rightarrow \left(H\text{-}Mn_3O_4\text{-}PEI\text{-}PtNPs\text{-}Ru(II)\right)_n\text{-}Eu^{3+} + h\nu \quad (4)$$

With the potential scanning from 0.2 to 1.25 V, both the luminophore and coreactant in the composite of $(H\text{-}Mn_3O_4\text{–}PEI\text{–}PtNPs\text{–}Ru(II))_n\text{–}Eu^{3+}$ were oxidized. By adopting PtNPs to act as nanochannels for electron transfer and energy transmission, the strong oxidant intermediate $(H\text{-}Mn_3O_4\text{–}PEI^{\bullet}\text{–}PtNPs\text{–}Ru(III))_n\text{–}Eu^{3+}$ changed to the excited state $(H\text{-}Mn_3O_4\text{–}PEI\text{–}PtNPs\text{–}Ru^{*}(II))_n\text{–}Eu^{3+}$. Finally, the enhanced ECL emission was obtained with $(H\text{-}Mn_3O_4\text{–}PEI\text{–}PtNPs\text{–}Ru^{*}(II))_n\text{–}Eu^{3+}$ returning back to the ground state.

2.6. Detection of CA2 with the Proposed Biosensor

Under the optimized experimental conditions (Figure S4, Supporting Information), the quantitative measurement of the proposed ECL biosensor was explored. According to **Figure 5**, the ECL intensity increased with increasing concentration of CA2 (curve a–h). The inset of Figure 5 showed that the ECL intensity was linear with the logarithm of the CA2 concentration. The linear equation was $I = 2991.6 + 751.4 \log c$ (where I was the ECL intensity and c was the concentration of CA2), and the correlation coefficient was 0.9985. The linear range was from 0.001 to 100 ng mL^{-1} with a detection limit of 0.3 pg mL^{-1} ($S/N = 3$).

2.7. Selectivity, Stability, and Reproducibility of the Proposed Biosensor

Some interfering agents (Hb, 20 ng mL^{-1}; IgG, 20 ng mL^{-1}) were applied to evaluate the selectivity of the proposed biosensor. As shown in **Figure 6**A, the ECL signal of the biosensor incubating with IgG was similar to that of the blank sample. And no obvious changes were observed compared to the ECL of the mixture of CA2 (1 ng mL^{-1}) and different interfering agents to that obtained in the pure CA2 (1 ng mL^{-1}). All that indicated that the biosensor possessed good selectivity for CA2. Meanwhile, the stability of the ECL biosensor was assessed under consecutive cyclic potential scans (Figure 6B). The relative standard deviations

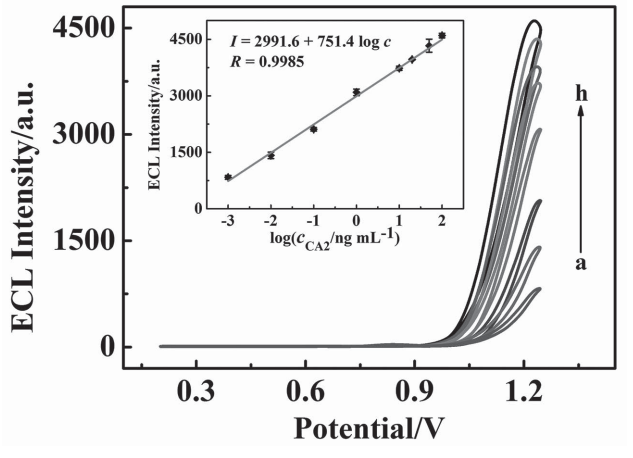

Figure 5. ECL profiles of the biosensor in the presence of different concentrations of CA2 a–h): 0.001, 0.01, 0.1, 1, 10, 20, 50, and 100 ng mL^{-1}. Inset: ECL calibration curve of the biosensor for CA2 determination. All ECL signals were measured in PBS (0.1 M, pH 7.4). The PMT was set at 800 V and the potential scan was from 0.2 to 1.25 V.

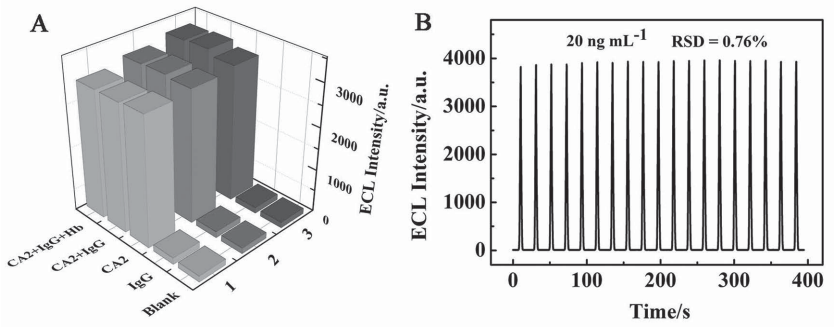

Figure 6. A) Comparison of ECL responses with different antigens: Blank; IgG (20 ng mL^{-1}); CA2 (1 ng mL^{-1}); a mixture containing CA2 (1 ng mL^{-1}) and IgG (20 ng mL^{-1}); a mixture containing CA2 (1 ng mL^{-1}), IgG (20 ng mL^{-1}), and Hb (20 ng mL^{-1}); B) The ECL stability of proposed biosensor under consecutive cyclic potential scans. All ECL signals were measured in PBS (0.1 M, pH 7.4). The PMT was set at 800 V and the potential scan was from 0.2 to 1.25 V.

(RSD) of 0.76% in 19 cycles suggested a good stability of the biosensor, which could be attributed to the excellent luminous stability of the self-enhanced electrochemiluminescent composite. In addition, the reproducibility of the proposed biosensor was estimated by the RSD (ECL response) of intra- and interassays that were not more than 5%, which implied that the reproducibility of the proposed biosensor was acceptable.

2.8. Application

To monitor the feasibility of the ECL biosensor, recovery experiments were explored in human serum by standard addition method. A series of target protein with different concentrations (defined as Added) was added into the human serum (diluted 50 times with PBS). Then, the proposed immunosensor was used to detect the target protein. Based on the obtained ECL intensity, the corresponding concentrations (defined as Found) of target protein were calculated according to the linear equation. The recovery was the ratio between the Found and Added. According to Table S1, Supporting Information, the recovery (between 91.16% and 109.4%) was obtained, which suggested that the proposed biosensor provided a potential tool for determining CA2 in real biological samples.

3. Conclusions

In conclusion, two specific peptides for selective recognition of CA2 are designed first. Then, Mn_3O_4 with hollow structure and good magnetic magnetism was synthesized using triblock copolymeric micelles as templates. Based on the obtained H-Mn_3O_4 and coordination of Eu^{3+}, sheet-like nanostructure ((H-Mn_3O_4–PEI–PtNPs–Ru)$_n$–Eu^{3+}) was prepared, which included the ECL luminophore and its coreactant in the same complex while PtNPs act as nanochannels for electron transfer between them. By this way, the luminous stability and efficiency had been greatly enhanced. The biosensor constructed based on the obtained nanostructures and the specific recognition of CA2-binding peptides had good response to CA2 in a wide linear range with outstanding selectivity, stability, and reproducibility. This work provided a new method for the construction of peptide biosensor and would extend the application of ECL in bioanalysis.

4. Experimental Section

Synthesis of PdNCs: PdNCs were synthesized according to our previous report.[24] First, 10 mL PVP (0.2 M) and 3.5 mL $AgNO_3$ (0.29 M) were successively added into 30 mL hot ethylene glycol. Silver nanocubes were obtained after heating, refluxing, and magnetic stirring at 160 °C for 40 min. By using the as-prepared silver nanocubes as templates, PdNCs were obtained through galvanic replacement reaction: K_2PdCl_4 (5 mL, 0.05 M) was added into the silver nanocubes solution (20 mL) with refluxing and heating for 40 min. At last, PdNCs were obtained by centrifugation and washing.

Preparation of H-Mn_3O_4 and the Sheet-Like Nanostructure: The preparation of H-Mn_3O_4 and (H-Mn_3O_4–PEI–PtNPs–Ru)$_n$–Eu^{3+} was showed in Scheme 2A. The micelle of PS-PVP-PEO was prepared according to the literature with some minor modifications.[36] First, 0.2 g of PS-PVP-PEO was dissolved in a mixture solution of water and *N*,*N*-dimethylformamide. After the PS-PVP-PEO polymer was completely dissolved, the solution was dialyzed against water to obtain the micelles of PS-PVP-PEO. The pH of the solution was adjusted to 10 with NaOH solution. Then, 0.5 g $Mn(Ac)_2$ was added. After the sol–gel reaction and drying at 50 °C, the obtained composites were calcined in a furnace at 500 °C for 4 h in air to remove the template polymer and obtain H-Mn_3O_4.

0.2 g H-Mn_3O_4 powder was dissolved in 5 mL distilled water. Then, 1 mL 3-aminopropyltrimethoxysilane (AMPTS) was added. With the assistance of glutaraldehyde (GA), PEI (1%) was decorated on the surface of H-Mn_3O_4. After magnetic separation and redispersion, 0.5 mL mixed solution of PtNPs and Ru(dcbpy)$_3^{2+}$ were added. The composite (H-Mn_3O_4–PEI–PtNPs–Ru) was obtained by magnetic separation, washing, and redispersion. Finally, $EuCl_3$ (0.5 mL, 0.01 M) was added into the solution of H-Mn_3O_4–PEI–PtNPs–Ru with stirring. After a few hours, the sheet-like nanostructure ((H-Mn_3O_4–PEI–PtNPs–Ru)$_n$–Eu^{3+}) was obtained by magnetic separation and redispersion. Due to the existence of the magnetic core (H-Mn_3O_4), all the unreacted reagents could be removed by magnetic separation.

Fabrication of the Peptide-Based ECL Biosensor: First of all, detection peptide (P_2) and T20 adsorbed (H-Mn_3O_4–PEI–PtNPs–Ru)$_n$–Eu^{3+} was prepared: 0.3 mL P_2 and 0.1 mL T20 were consecutively added into 2 mL solution of (H-Mn_3O_4–PEI–PtNPs–Ru)$_n$–Eu^{3+} with stirring. Then, the (H-Mn_3O_4–PEI–PtNPs–Ru)$_n$–Eu^{3+}@P_2-T20 bioconjugate was obtained by magnetic separation and redispersion.

The fabrication of the peptide-based ECL biosensor was schematized in Scheme 2B. The GCE (ϕ = 4 mm) was polished successively with 0.3, 0.05 μm alumina slurry and sonicated for 2 min before modification. The cleaned GCE was first coated with

5 μL PdNCs dispersed with chitosan (Chi, 0.6%) solution. After drying, 16 μL capture peptide (P_1) was dropped onto the electrode with incubating for 8 h. Then, the modified electrode was immersed into the solution of T20 for preventing the nonspecific binding. Subsequently, the resulted electrode was incubated in CA2 solution for 50 min. Finally, with a sandwich recognition format, 16 μL (H-Mn_3O_4–PEI–PtNPs–Ru)$_n$–Eu^{3+}@P_2-T20 solution was dropped onto the as-prepared electrode. Especially, based on the excellent magnetic properties, the bioconjugate of (H-Mn_3O_4–PEI–PtNPs–Ru)$_n$–Eu^{3+}@P_2-T20 could be used cyclically through magnetic detachment.

Supporting Information

Supporting Information is available from the Wiley Online Library or from the author.

Acknowledgements

This work was financially supported by the NNSF of China (51473136, 21275119), Fundamental Research Funds for the Central Universities (XDJK2014C138), and China Postdoctoral Science Foundation (2014M550454).

[1] F. N. Xiao, M. Wang, F. B. Wang, X. H. Xia, *Small* **2014**, *10*, 706.
[2] J. Hu, T. Wang, J. Kim, C. Shannon, C. J. Easley, *J. Am. Chem. Soc.* **2012**, *134*, 7066.
[3] R. A. Abuknesha, F. Jeganathan, J. Wu, Z. Baalawy, *Nat. Protoc.* **2009**, *4*, 452.
[4] H. Orelma, T. Teerinen, L. Johansson, S. Holappa, J. Laine, *Biomacromolecules* **2012**, *13*, 1051.
[5] J. M. Chalker, G. J. L. Bernardes, B. G. Davis, *Acc. Chem. Res.* **2011**, *44*, 730.
[6] M. Mascini, I. Palchetti, S. Tombelli, *Angew. Chem., Int. Ed.* **2012**, *51*, 1316.
[7] H. Li, H. Xie, Y. Cao, X. Ding, Y. Yin, G. Li, *Anal. Chem.* **2012**, *85*, 1047.
[8] J. H. Collier, T. Segura, *Biomaterials* **2011**, *32*, 4198.
[9] C. Katz, L. Levy-Beladev, S. Rotem-Bamberger, T. Rito, S. G. D. Rudigerb, S. Friedler, *Chem. Soc. Rev.* **2011**, *40*, 2131.
[10] H. N. Xie, H. Li, Y. Huang, X. Y. Wang, Y. M. Yin, G. X. Li, *ACS Appl. Mater. Interfaces* **2014**, *6*, 459.
[11] G. F. Gui, Y. Zhuo, Y. Q. Chai, Y. Xiang, R. Yuan, *Anal. Chem.* **2014**, *86*, 5873.
[12] F. Girard, U. Strausfeld, A. Fernandez, N. J. Lamb, *Cell* **1991**, *67*, 1169.
[13] T. Y. Kim, W. G. Kaelin Jr., *Mol. Biol. Cell* **2001**, *12*, 2207.
[14] C. Liao, S. Q. Li, X. Wang, S. Muhlrad, A. Bjartell, D. J. Wolgemuth, *Int. J. Cancer* **2004**, *108*, 654.
[15] C. H. Yam, T. K. Fung, R. Y. Poom, *Cell. Mol. Life Sci.* **2002**, *59*, 1317.
[16] N. Mendoza, S. Fong, J. Marsters, H. Koeppen, R. Schwall, D. Wickramasinghe, *Cancer Res.* **2003**, *63*, 1020.
[17] E. Pazos, D. Torrecilla, M. V. López, L. Castedo, J. L. Mascareñas, A. Vidal, M. E. Vázquez, *J. Am. Chem. Soc.* **2008**, *130*, 9652.
[18] L. Y. Feng, L. Wu, J. S. Wang, J. S. Ren, D. Miyoshi, N. Sugimoto, X. G. Qu, *Adv. Mater.* **2012**, *24*, 125.
[19] L. Zhang, W. X. Niu, W. Y. Gao, L. M. Qi, J. P. Lai, J. M. Zhao, G. B. Xu, *ACS Nano* **2014**, *8*, 5953.
[20] H. L. Qi, X. Y. Qiu, D. P. Xie, C. Ling, Q. Gao, C. X. Zhang, *Anal. Chem.* **2013**, *85*, 3886.
[21] L. Wu, J. S. Wang, M. L. Yin, J. R. Ren, D. Miyoshi, N. Sugimoto, X. G. Qu, *Small* **2014**, *10*, 330.
[22] S. Y. Deng, L. X. Cheng, J. P. Lei, Y. Cheng, Y. Huang, H. X. Ju, *Nanoscale* **2013**, *5*, 5435.
[23] N. Hao, X. L. Li, H. R. Zhang, J. J. Xu, H. Y. Chen, *Chem. Commun.* **2014**, *50*, 14828.
[24] H. J. Wang, L. J. Ba, Y. Q. Chai, R. Yuan, *Small* **2014**, *10*, 1857.
[25] L. Z. Hu, G. B. Xu, *Chem. Soc. Rev.* **2010**, *39*, 3275.
[26] M. S. Wu, D. J. Yuan, J. J. Xu, H. Y. Chen, *Anal. Chem.* **2013**, *85*, 11960.
[27] H. J. Wang, Y. He, Y. Q. Chai, R. Yuan, *Nanoscale* **2014**, *6*, 10316.
[28] K. Yang, G. B. Yang, L. Chen, L. Cheng, L. Wang, C. C. Ge, Z. Liu, *Biomaterials* **2015**, *38*, 1.
[29] Y. Zhou, Y. Zhuo, N. Liao, Y. Q. Chai, R. Yuan, *Chem. Commun.* **2014**, *50*, 14627.
[30] J. B. Joo, I. Lee, M. Dahl, *Adv. Mater.* **2013**, *23*, 4246.
[31] X. Q. Huang, Y. J. Li, Y. Chen, E. Zhou, Y. X. Xu, H. L. Zhou, X. F. Duan, Y. Huang, *Angew. Chem. Int. Ed.* **2013**, *52*, 2520.
[32] J. E. Cloud, K. McCann, K. A. P. Perera, Y. A. Yang, *Small* **2013**, *9*, 2532.
[33] Y. Sun, Y. Xia, *Science* **2002**, *298*, 2176.
[34] Y. G. Sun, Y. N. Xia, *J. Am. Chem. Soc.* **2004**, *126*, 3892.
[35] S. E. Skrabalak, J. Y. Chen, Y. G. Sun, X. M. Lu, L. Au, C. M. Cobley, Y. N. Xia, *Acc. Chem. Res.* **2008**, *41*, 1587.
[36] A. Khanal, Y. Inoue, M. Yada, K. Nakashima, *J. Am. Chem. Soc.* **2007**, *129*, 1534.
[37] M. Sasidharan, K. Nakashima, *Acc. Chem. Res.* **2014**, *47*, 157.

Received: February 2, 2015
Revised: March 7, 2015
Published online: April 2, 2015

